Catalytic conversion reactions in nanoporous systems with concentration-dependent selectivity: Statistical mechanical modeling

Andrés García,[1,2] Jing Wang,[1,3,*] Theresa L. Windus,[1,4] Aaron D. Sadow,[1,4] and James W. Evans[1,2,3]
[1]*Ames Laboratory–USDOE, Iowa State University, Ames, Iowa 50011, USA*
[2]*Department of Physics & Astronomy, Iowa State University, Ames, Iowa 50011, USA*
[3]*Department of Mathematics, Iowa State University, Ames, Iowa 50011, USA*
[4]*Department of Chemistry, Iowa State University, Ames, Iowa 50011, USA*
(Received 26 January 2016; published 20 May 2016)

Statistical mechanical modeling is developed to describe a catalytic conversion reaction $A \to B^c$ or B^t with concentration-dependent selectivity of the products, B^c or B^t, where reaction occurs inside catalytic particles traversed by narrow linear nanopores. The associated restricted diffusive transport, which in the extreme case is described by single-file diffusion, naturally induces strong concentration gradients. Furthermore, by comparing kinetic Monte Carlo simulation results with analytic treatments, selectivity is shown to be impacted by strong spatial correlations induced by restricted diffusivity in the presence of reaction and also by a subtle clustering of reactants, A.

DOI: 10.1103/PhysRevE.93.052137

I. INTRODUCTION

Molecular-level nonequilibrium statistical mechanical modeling has the potential to provide a reliable description of cooperative catalytic reaction-diffusion phenomena where traditional mean-field (MF) treatments of chemical kinetics are inadequate [1,2]. The focus of this paper is on providing such a treatment of catalytic systems with two distinctive features. The *first* involves solution-phase first-order $A \to B$ conversion reactions occurring in catalytically functionalized particles traversed by narrow linear nanopores which result in restricted diffusive transport [3–11]. The extreme case of restricted transport, on which we place some emphasis here, is single-file diffusion (SFD) [12–14] wherein reactant and product species cannot pass each other within the linear nanopores. Then the interplay between reaction and SFD produces rapidly varying concentration profiles near the pore openings (where the reactant is supplied from the surrounding fluid), and strong spatial correlations in reactant locations. The latter are neglected in MF treatments. The *second* phenomenon involves reactions with concentration-dependent selectivity, and specifically stereoselectivity where the product B can have distinct cis (B^c) and trans (B^t) forms [15]. Here, the selection of the B^c or B^t product is controlled by the concentration of the reactant, A. More precisely, in a molecular-level picture, the rate for conversion of A to B^c or B^t depends on the number and local arrangement of other nearby A species. This, in turn, means that the selectivity, i.e., the relative yield of each of these products, depends on spatial correlations in the reactant distribution.

Characteristic indicators of SFD in catalytic mesoporous systems were observed long ago for certain classes of zeolites with uncoupled narrow linear pores [16,17]. It should, however, also be noted that in samples with linear dimensions of tens of microns, these uncoupled pores may not traverse the entire sample [18]. A primary motivation for our study is catalytic processes in functionalized mesoporous silica nanoparticles (MSNs) with diameters of around 100–200 nm where hexagonal arrays of parallel uncoupled linear nanopores do traverse the entire nanoparticle [19]. While synthesis with a range of pore diameters is possible, the broadest of which certainly allows uninhibited transport, recent studies for narrow pores did reveal behavior indicative of SFD [2,20].

There has been extensive characterization of spatial correlations of thermodynamic origin associated with intermolecular interactions in equilibrium systems. However, understanding of spatial correlations of kinetic origin in the nonequilibrium steady states of reaction-diffusion systems is limited [1,2]. Nonetheless, it is precisely the characterization of such nonequilibrium correlations which is required for reliable prediction of selectivity and other features of concentration-dependent stereoselective reactions in nanoporous systems. Given the fundamental nature of this challenge, it is addressed here with somewhat simplified statistical mechanical models, as described in detail below. We note that over the last two decades a substantial body of analysis based on such models has been performed for conversion reactions in nanoporous systems (usually zeolites) with simple concentration-independent first-order kinetics [3–11]. One can straightforwardly extend this type of modeling to incorporate cooperative concentration-dependent kinetics, but it will prove a significant challenge to provide a reliable analytic treatment.

Our focus is on such simplified and generic modeling. However, here we first provide some brief comments for broader background and motivation regarding the type of systems falling into the above class and also on theoretical methodologies with the potential to provide a first-principles characterization of reaction kinetics. With regard to concentration-dependent selectivity, homogeneous catalytic desymmetrization of diallylamines to give diastereomers (using a Zr-centered catalyst) exhibits a quite strong variation with reactant concentration of cis to trans selectivity [15]. Specifically, the yield of trans relative to cis product increases with reactant concentration. These studies are part of a broader analysis of stereoselectivity in Zr catalyzed reactions [15,21]. To develop a heterogeneous version of this process, one might

*Current address: American Institutes for Research, 1000 Thomas Jefferson St. NW, Washington, DC 20007, USA.

anticipate functionalizing the interior pore surfaces of MSN with an appropriate Zr-centered catalytic group. The effective diameter of the pores after functionalization can be reduced to the range of $d \sim 1-2$ nm where passing of molecular species within the pore can be strongly inhibited. While such functionalization remains a significant challenge, substantial progress has been made recently [22].

Next, we remark that electronic structure analysis could provide a detailed theoretical assessment of the origin and nature of concentration-dependent selectivity. More specifically, such analysis should ideally elucidate variations in reaction barriers and possibly also pathways with the local environment of the reacting "substrate" molecule A. This is a significant challenge even for homogeneous catalytic systems, but one might anticipate that the basic features are preserved for heterogeneous catalytic analogues. Given the typical complexity and size of the catalytic group, and the requirement to incorporate multiple reactant molecules, it is natural to utilize computationally less expensive density functional theory (DFT) to facilitate such an analysis rather than higher-level quantum chemistry approaches. Indeed, this type of analysis has been performed for systems similar to that described above and has demonstrated that certain barriers can indeed be lowered by increasing the number of reactant molecules [23]. Current analysis has not included solvent effects, but this could be done explicitly or using implicit solvent approaches such as COSMO [24] or PCM [25]. It is also appropriate to note that once geometries along the reaction path have been determined by DFT, higher-level analyses such as MP2 and CCSD can be implemented utilizing those geometries to assess corrections to the energetics. In one case, the MP2 calculations yielded similar energetics to the DFT analysis [23].

Returning to statistical mechanical modeling, we briefly review an effective strategy utilized in previous studies to describe solution-phase catalytic conversion reactions with restricted transport within catalytically functionalized linear nanopores. Direct molecular or Langevin dynamics simulation [26–28] is not viable to describe the overall reaction-diffusion process on the appropriate time scale (i.e., reactants entering, diffusing within, reacting, and products diffusing within and being extruded from the pore, with dynamics generally mediated by the presence of a solvent). Thus, instead spatially discrete coarse-grained stochastic modeling is typically implemented [3–11]. In this approach, each pore is divided into a linear array of cells each with width $a \sim 1$ nm comparable to that of the reactant and product species. Then solvent-mediated diffusion is described by hopping to adjacent empty cells. Refinements can be made to relax the SFD constraint. Adsorption and desorption from the pore are reflected in appropriate boundary conditions at the pore openings. A conversion reaction will be analyzed here with rates which reflect the local environment of the cell where reaction is occurring. The behavior of the stochastic one-dimensional lattice-gas model is precisely assessed by kinetic Monte Carlo (KMC) simulation [2]. However, for a deeper understanding, one can develop exact master equations for the model. Although these cannot be solved exactly, and standard mean-field type treatments are inadequate, effective analytic treatments such as a generalized hydrodynamic (GH) approximation [10] might be developed to elucidate behavior.

In Sec. II, we develop a spatially discrete stochastic model for catalytic conversion $A \to B^c$ or B^t in nanopores with restricted transport, present the exact evolution equations, and comment on an effective analytic treatment of diffusion. Section III provides a characterization of the key spatial correlations in the steady state of the nonequilibrium reaction-diffusion system, focusing on the reactant distribution and elucidating the strong correlations which impact the diffusion fluxes. In Sec. IV, we present an analysis of model behavior, specifically describing nontrivial concentration profiles in the steady state and elucidating the key features impacting the selectivity. Conclusions are provided in Sec. V.

II. MODEL SPECIFICATION AND EVOLUTION EQUATIONS

A. Specification of the spatially discrete stochastic model

Spatially discrete modeling describes catalytically functionalized nanoporous particles, such as MSN, by an ensemble of linear pores each consisting of a 1D array of L cells, labeled $n = 1 - L$, each of width $a \sim 1$ nm [3–11]. In our treatment, all cells are regarded as catalytically active. It is convenient to consider these 1D arrays as being extended to a 3D array of cells in the exterior fluid surrounding the catalytic particles as this facilitates specification of adsorption and desorption processes at the pore ends. The exterior fluid supplies reactant, A, to the pores, and we consider here only the initial stage of the reaction where a negligible fraction of the reactant in the external fluid has been converted to product. We consider the conversion reaction $A \to B^c$ or B^t occurring exclusively inside the pores, as indicated above, and let E denote empty cells. It will also be useful to let $B = B^c + B^t$ denote either product, $X = A + B$ denote any type of species, and $Z = B + E$ denote cells not populated by A. Also if $C = A$, B^c, or B^t, then we will let C' denote other molecular species, e.g., if $C = A$ then $C' = B$.

The probability that site n is occupied by some species C, corresponding to a concentration at site n, is denoted by $\langle C_n \rangle$, where $0 \leqslant \langle C_n \rangle \leqslant 1$. Similarly, the pair probability that site n is occupied by C and $n+1$ by D is denoted by $\langle C_n D_{n+1} \rangle$, etc. The "well-stirred" exterior fluid has a large volume compared to the intrapore region. For the initial stages of the reaction under consideration, we specify that a fixed fraction, $\langle A_0 \rangle = \langle X_0 \rangle$ of cells in the exterior fluid are randomly populated by reactant A. Thus, the fraction of exterior empty cells is given by $\langle E_0 \rangle = 1 - \langle X_0 \rangle$. As an aside, one can regard efficient stirring of the exterior fluid as corresponding to very rapid hopping of A between adjacent exterior cells.

The key ingredients of our stochastic model for the catalytic reaction-diffusion process, shown schematically in Fig. 1, are as follows:

(i) Reactants A "adsorb" at rate h from the fluid cell just outside the pore to empty end cells $n = 1$ and $n = L$. Thus, the overall rate to adsorb, e.g., at the left end of the pore is $h\langle A_0 \rangle \langle E_1 \rangle$ accounting for the feature there is no correlation between the occupancy of the exterior and interior cells.

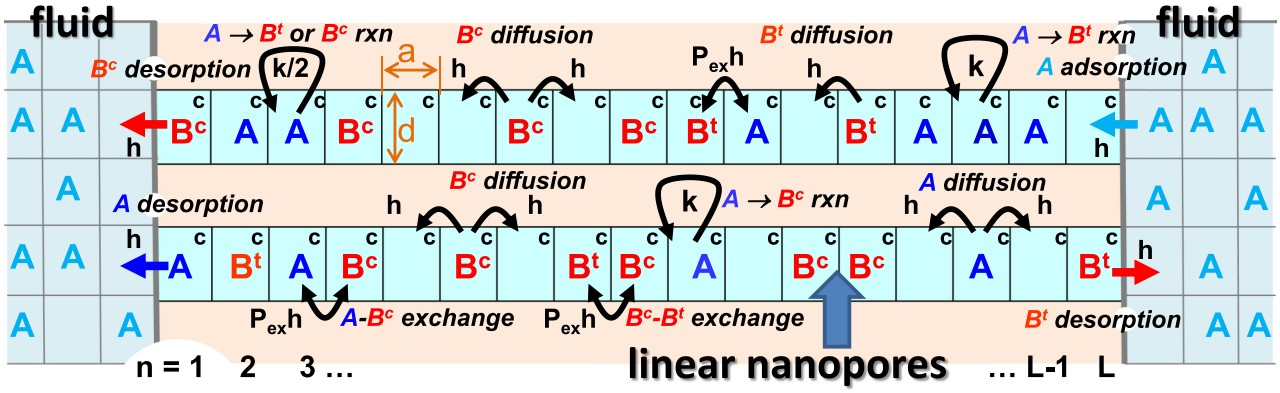

FIG. 1. Schematic of spatially discrete stochastic reaction model for concentration-dependent conversion reaction $A \to B^c$ or B^t in catalytically functionalized linear nanopores described by a 1D array of cells.

(ii) Reactants A hop at rate h to nearest-neighbor (NN) empty cells within the pore.

(iii) Reactants A convert to products B^c or B^t with rates depending on the local environment, specifically the state of the neighboring cells, as prescribed below.

(iv) Both types of product also hop at rate h to NN empty sites within the pore.

(v) Reactants and products "desorb" by hopping from end cells at rate h to NN empty cells in the surrounding fluid. Thus, e.g., the overall rate for A to desorb from the left end of the pore is $h\langle A_1\rangle\langle E_0\rangle$.

(vi) One can relax the SFD constraint implicit in the above prescription of hopping by simply allowing exchange of adjacent (NN) species within the pore with rate $P_{\rm ex}h$. Of key impact is exchange of reactants and products. Selecting $P_{\rm ex} = 0$ recovers SFD (for narrow pores), and setting $P_{\rm ex} = 1$ corresponds to uninhibited passing (for wide pores).

It is appropriate to note that since we focus on the initial stage of the reaction, the extruded product is extremely diluted in the well-stirred fluid and does not readasorb. Also, we remark that the assignment of equal hop rates is natural for cis and trans products, and this is also reasonable for reactants for the type of reaction mentioned in Sec. I which motivates this study.

Our primary aim of incorporating concentration-dependent selectivity, or more precisely environment-dependent selectivity, is achieved by specifying that the rate for conversion of A at cell n depends on the state of neighboring cells as follows:

$$A_{n-1}\,A_n\,A_{n+1} \to A_{n-1}\,B_n^t\,A_{n+1} \text{ at rate } k, \tag{1a}$$

$$A_{n-1}\,A_n\,Z_{n+1} \to A_{n-1}\,B_n^c\,Z_{n+1} \text{ or } A_{n-1}\,B_n^t\,Z_{n+1} \text{ each at rate } k/2, \tag{1b}$$

$$Z_{n-1}\,A_n\,A_{n+1} \to Z_{n-1}\,B_n^c\,A_{n+1} \text{ or } Z_{n-1}\,B_n^t\,A_{n+1} \text{ each at rate } k/2, \tag{1c}$$

$$\text{and} \quad Z_{n-1}\,A_n\,Z_{n+1} \to Z_{n-1}\,B_n^c\,Z_{n+1} \text{ at rate } k, \tag{1d}$$

where again Z means *not* A. Using exact "conservation of probability" relations, the above prescription implies that the rate of loss by reaction of A at site n equals $R_n(A) = -k\langle A_n\rangle$. Likewise, the rates of gain by reaction of specific products at site n are given by

$$R_n(B^t) = \tfrac{1}{2}k\,(\langle A_n A_{n+1}\rangle + \langle A_{n-1}A_n\rangle)$$
$$\text{and} \quad R_n(B^c) = \tfrac{1}{2}k(\langle A_n\,Z_{n+1}\rangle + \langle Z_{n-1}A_n\rangle), \tag{2}$$

where $R_n(B^c)$ can be rewritten using $\langle A_n Z_{n+1}\rangle = \langle A_n\rangle - \langle A_n A_{n+1}\rangle$, etc. Clearly, the overall gain of products satisfies $R_n(B) = R_n(B^c) + R_n(B^t) = -R_n(A)$.

This model has the following special features. Ignoring the distinction between B^c and B^t, the model reduces exactly to a simple concentration-independent conversion model $A \to B$ with rate k for all cells. Thus, the concentration profile for A (which decays quickly into the pore), and all spatial correlations in the location of A species in the full $A \to B^c$ or B^t model, are determined by this simpler $A \to B$ model. If one does not distinguish A and B, then the model reduces to a simple nonreactive diffusion model for a single species X. Thus, the steady state corresponds to a random distribution of X in cells within the pore with uniform concentration, $\langle X_n\rangle = \langle X_0\rangle$. A corollary of this observation is that empty cells are also distributed randomly in the steady state with uniform concentration $\langle E_n\rangle = 1 - \langle X_0\rangle = \langle E_0\rangle$.

Finally, we note that the above modeling can be refined or extended in various ways. For example, the SFD constraint could instead be relaxed by modeling pores as consisting of multiple parallel rows of cells [2] (rather than by including place exchange for pores with a single row of cells). Also, rather than just considering the initial stages of reaction where a negligible fraction of reactant in the fluid is converted to product, one can also assess reactivity for various degrees, f, of conversion of reactant to products. Here one exploits an assumed separation-of-time-scales feature that a quasi-steady state within pores will be quickly achieved for each f relative to the time scale for conversion of most reactant to product in the fluid. Thus, from an analysis of reactivity for a series of f values, one can piece together overall reaction kinetics [11].

B. KMC simulation and master equation analysis

Precise analysis of model behavior will be achieved by kinetic Monte Carlo (KMC) simulations, some details of which are described in Appendix A. However, potentially deeper insight comes from an analytic treatment based on exact evolution equations for the $A \to B^c$ or B^t model, which

can be written in compact form:

$$d/dt\langle C_n\rangle = R_n(C) - \nabla_n J_C(n > n+1),$$
$$\text{for } 1 < n < L \text{ with } C = A,\ B^c, \text{ or } B^t. \quad (3)$$

Here $\nabla_n K_n = K_n - K_{n-1}$ denotes a discrete gradient, and the net diffusion flux, $J_C(n > n+1)$, of C from cell n to cell $n+1$ satisfies [10]

$$J_C(n > n+1) = h(\langle C_n E_{n+1}\rangle - \langle E_n C_{n+1}\rangle) + P_{\rm ex}\, h(\langle C_n C'_{n+1}\rangle - \langle C'_n\, C_{n+1}\rangle). \quad (4)$$

Separate equations are needed for end cells which reflect the feature that the cell just outside the pore is randomly populated by A with probability $\langle X_0\rangle$. Thus, pair probabilities involving the end cell and the adjacent exterior cell factorize as a product of single-cell probabilities, e.g., $d/dt\langle A_1\rangle = R_1(A) - J_A(1 > 2) + h(\langle A_0\rangle\langle E_1\rangle - \langle E_0\rangle\langle A_1\rangle)$.

All these equations couple single-cell probabilities to pair probabilities. One can develop separate equations for pair probabilities [2], e.g.,

$$\begin{aligned} d/dt\langle A_n\, A_{n+1}\rangle &= -2k\langle A_n\, A_{n+1}\rangle - h(\langle A_n A_{n+1} E_{n+2}\rangle \\ &\quad - \langle A_n E_{n+1} A_{n+2}\rangle) + h(\langle A_{n-1} E_n A_{n+1}\rangle \\ &\quad - \langle E_{n-1} A_n A_{n+1}\rangle) - P_{\rm ex}\, h(\langle A_n A_{n+1} A'_{n+2}\rangle \\ &\quad - \langle A_n\, A'_{n+1}\, A_{n+2}\rangle) + P_{\rm ex}\, h(\langle A_{n-1} A'_n\, A_{n+1}\rangle \\ &\quad - \langle A'_{n-1}\, A_n\, A_{n+1}\rangle), \end{aligned} \quad (5)$$

for $1 < n < L-1$ which couple to triplet probabilities. Continuing to develop equations for triplets, etc., generates a hierarchy of evolution equations.

The simplest mean-field (MF) treatment completely neglects spatial correlations by factorizing all multicell probabilities as products of single-cell quantities. However, for the $A \to B$ conversion reaction, this MF treatment has been shown to greatly overestimate the magnitude of the diffusion flux terms, $J_C(n > n+1)$, for SFD, and thus overestimates reactant penetration into the pore and reactivity in the steady state for $k \ll h$ [9,10]. This is perhaps not surprising as it is well recognized that there are strong back correlations in hop sequences associated with SFD [14]. Of course, the MF treatment also neglects correlations determining $\langle A_n A_{n+1}\rangle$ pair probabilities which will be important for accurate description of reaction kinetics. The pair approximation sets $\langle C_n D_{n+1} F_{n+2}\rangle \approx \langle C_n D_{n+1}\rangle\langle D_{n+1} F_{n+2}\rangle/\langle D_{n+1}\rangle$ attempting to account for spatial correlations, and requires simultaneous analysis of equations for both single-cell and pair probabilities. This yields somewhat improved results, but still significantly overestimates fluxes for $k \ll h$, as do higher-order triplet, etc., approximations [10].

The deficiency of MF-type approximations in describing diffusion fluxes has been remedied by implementing a generalized hydrodynamic (GH) treatment [10] of diffusion for the relevant counter-diffusion modes [29] where the total concentration $\langle X_n\rangle = \langle X_0\rangle$ is constant. Here we start with a hydrodynamic expression for diffusion fluxes $J_C(n > n+1) = -D_{\rm tr}\nabla_n\langle C_{n+1}\rangle$ which is applicable for counter diffusion and involves a tracer diffusion coefficient, $D_{\rm tr}$ [2,10,29–31]. Then, we replace the hydrodynamic $D_{\rm tr}$, which equals zero for SFD in an infinite pore, by a GH form $D_{\rm tr}(n, n+1) = h\, F_{\rm tr}(n, n+1)$. This GH form has a finite value $O(1/L)$ in the pore center and is enhanced near the pore openings [10]. Then the diffusion flux is given in this GH formulation by

$$J_C(n > n+1) \approx -h\, F_{\rm tr}(n,n+1)\, \nabla_n\langle C_{n+1}\rangle. \quad (6)$$

As described in detail elsewhere [2,10,29], $F_{\rm tr}(n,n+1))$ are determined either from the form of concentration profiles for a counter-permeation setup, or by suitable analysis of tagged particle diffusion with various starting locations. Illustrative values for $F_{\rm tr}(n,n+1)$ will be given below. This analysis produces a diffusion flux which is far smaller in magnitude than the MF prediction for SFD. Additional perspective on this feature comes from the observation that the MF value of $F_{\rm tr}$ is given by

$$F_{\rm tr}({\rm MF}) = \langle E_0\rangle + P_{\rm ex}\langle X_0\rangle. \quad (7)$$

See Appendix B. For SFD with $P_{\rm ex} = 0$, we will find that $F_{\rm tr}(n,n+1)$ is well below $F_{\rm tr}({\rm MF}) = \langle E_0\rangle$. We discuss further the implications of the success of the GH treatment in Sec. III.

The regime where spatial correlations are strongest and where analytic treatment most challenging is for $P_{\rm ex} = 0$ (SFD) with higher values of $\langle X_0\rangle$ and $k \ll h$. Higher $\langle X_0\rangle$ amplifies the constraints of SFD, and $k \ll h$ produces substantial reactant penetration to the pore so the form of the concentration profile impacted strongly by SFD. Thus, our discussion will particularly emphasize the case $P_{\rm ex} = 0$, $\langle X_0\rangle = 0.8$, and $k/h = 0.001$, choosing a pore length $L = 100$. Spatial correlations are reduced upon allowing exchange or reducing $\langle X_0\rangle$, so any treatment which is effective for $P_{\rm ex} = 0$ and high $\langle X_0\rangle$ will be even more accurate for $P_{\rm ex} > 0$ and lower $\langle X_0\rangle$. We will also consider behavior for $\langle X_0\rangle = 0.2$ and $P_{\rm ex} = 0.25$ confirming this feature. Likewise, for larger k, significant reactant concentration is limited to near pore openings where correlations are weaker, and thus lower-level approximations are more effective [2].

Our most successful analytic treatment, described as an "extended GH" or eGH approach, will incorporate a GH treatment of diffusion fluxes with a tailored treatment of spatial correlations in the pair quantities, $\langle A_n A_{n+1}\rangle$, which control the reaction kinetics $R_n(C)$. See Sec. III for details of the latter.

III. SPATIAL CORRELATIONS IN THE REACTIVE STEADY STATE

A. Correlations related to diffusion fluxes

The dramatic failure of the MF treatment of diffusion fluxes for SFD, which is reflected in the inequality $F_{\rm tr}(n, n+1) \ll F_{\rm tr}({\rm MF}) = \langle E_0\rangle$, implies strong spatial correlations between the location of cells which are empty and those which are populated by reactants, A, within the pore. This behavior is quantified by the GH formulation (6) which shows that

$$\langle A_n E_{n+1}\rangle - \langle E_n A_{n+1}\rangle \approx F_{\rm tr}(n,n+1)(\langle A_n\rangle - \langle A_{n+1}\rangle) \ll \langle E_o\rangle(\langle A_n\rangle - \langle A_{n+1}\rangle), \quad (8)$$

where these quantities are positive near the left end of the pore, and where illustrative values for $F_{\rm tr}(n,n+1)$ are given in Table I. Thus, as is shown in Fig. 2 for SFD with $\langle X_0\rangle = 0.8$ and $k/h = 0.001$, $\langle A_n E_{n+1}\rangle$ and $\langle E_n A_{n+1}\rangle$ are

TABLE I. $F_{tr}(n, n+1)$ versus n near the end of a pore with $L = 100$ for different values of total concentration $\langle X_0\rangle$ and for SFD ($P_{ex} = 0$) as well as with exchange ($P_{ex} = 0.25$). Decay into the pore (increasing n) is strong for SFD and weak with exchange. MF values, $F_{tr}(\text{MF}) = 1 - (1 - P_{ex})\langle X_0\rangle$ are shown in the bottom row. $F_{tr}(n, n+1)$ is closest to $F_{tr}(\text{MF})$ for low $\langle X_0\rangle$ and $P_{ex} > 0$, and furthest below $F_{tr}(\text{MF})$ for high $\langle X_0\rangle$ and $P_{ex} = 0$.

$F_{tr}(n,n+1)$	$\langle X_0\rangle = 0.20$, $P_{ex} = 0.00$	$\langle X_0\rangle = 0.20$, $P_{ex} = 0.25$	$\langle X_0\rangle = 0.80$, $P_{ex} = 0.00$	$\langle X_0\rangle = 0.80$, $P_{ex} = 0.25$
$n = 1$	0.59353	0.76127	0.05463	0.32147
$n = 2$	0.43812	0.71861	0.02302	0.31004
$n = 3$	0.35470	0.69915	0.01295	0.30757
$n = 4$	0.27708	0.68507	0.00865	0.30522
$n = 5$	0.23021	0.69082	0.00627	0.30112
$n = 6$	0.19527	0.66456	0.00494	0.30126
$n = 7$	0.16801	0.66701	0.00411	0.29957
$n = 8$	0.15003	0.66144	0.00358	0.29984
$n = 9$	0.13627	0.66434	0.00327	0.29802
$n = 10$	0.12136	0.65669	0.00304	0.29793
$n = 11$	0.10895	0.65478	0.00286	0.29734
$n = 12$	0.09805	0.64189	0.00274	0.29869
$n = 13$	0.09060	0.64692	0.00265	0.29780
$n = 14$	0.08285	0.64900	0.00260	0.29823
$n = 15$	0.07682	0.64390	0.00255	0.29618
$F_{tr}(\text{MF})$	0.80	0.85	0.20	0.40

much closer to each other than the MF predictions. (The large difference between the MF estimates reflects a strong variation in $\langle A_n\rangle$ near the pore opening, noting that $\langle E_n\rangle = \langle E_0\rangle$ is constant.) The similarity of $\langle A_n E_{n+1}\rangle$ and $\langle E_n A_{n+1}\rangle$ is readily understood as a consequence of the restricted dynamics associated with SFD. Consider the pair probability $\langle A_n E_{n+1}\rangle$. Since cell $n+1$ is empty, A on cell n can readily hop to cell $n+1$ and will then quite likely hop back to cell n (which is guaranteed to be empty immediately after A hopping). This results in a "near-equalization" of the probabilities $\langle A_n E_{n+1}\rangle$ and $\langle E_n A_{n+1}\rangle$. This idea naturally extends to triplets

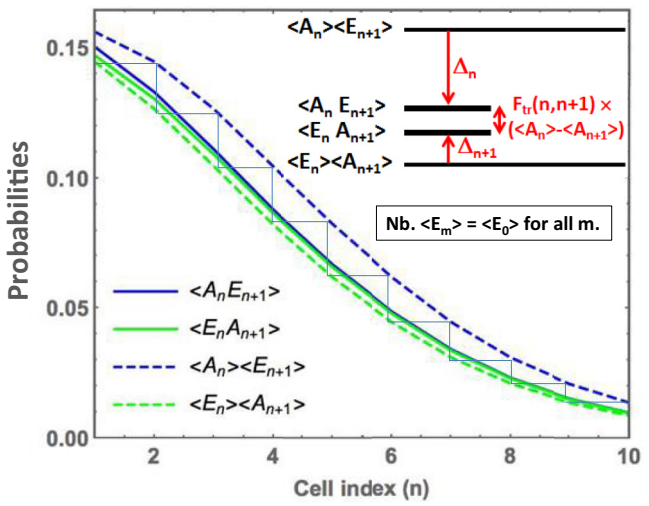

FIG. 2. KMC results for behavior of $\langle A_n E_{n+1}\rangle$ and $\langle E_n A_{n+1}\rangle$ (solid curves) relative to their MF approximations (dashed curves) versus n near the left end of a pore with $L = 100$, $\langle X_0\rangle = 0.8$ (so $\langle E_0\rangle = 0.2$), $k/h = 0.001$, and $P_{ex} = 0$ (SFD). Since $\langle E_n\rangle = \langle E_0\rangle$, both MF approximations are determined solely by the variation of $\langle A_n\rangle$ with n (as reflected in the "staircase" construction connecting dashed curves).

$\langle A_n E_{n+1} E_{n+2}\rangle$, $\langle E_n A_{n+1} E_{n+2}\rangle$, and $\langle E_n E_{n+1} A_{n+2}\rangle$ which are much closer to each other than the MF values, and also extends to associated quartets, quintets, etc.

The GH formulation only quantifies the difference between the pair probabilities as indicated in (8). However, it will be useful to also have reliable estimates of the individual probabilities $\langle A_n E_{n+1}\rangle$ and $\langle E_n A_{n+1}\rangle$. To this end, we introduce an extended GH or eGH approximation as follows. First, we note the anticipated inequality

$$\langle A_n\rangle\langle E_0\rangle = \langle A_n\rangle\langle E_{n+1}\rangle > \langle A_n\, E_{n+1}\rangle > \langle E_n A_{n+1}\rangle > \langle E_n\rangle\langle A_{n+1}\rangle = \langle E_0\rangle\langle A_{n+1}\rangle, \tag{9}$$

for the left end of the pore (smaller n) which is confirmed by the results in Fig. 2. One approach to assess $\langle A_n E_{n+1}\rangle$ and $\langle E_n A_{n+1}\rangle$ accounts for a "strong asymmetry" in the behavior of these quantities relative to MF predictions in that both are much closer to $\langle E_n\rangle\langle A_{n+1}\rangle$ than to $\langle A_n\rangle\langle E_{n+1}\rangle$ for SFD with high $\langle X_0\rangle$ (or low $\langle E_0\rangle$) [32]. In the notation of the inset to Fig. 2, this suggests setting $\Delta_{n+1} = 0$ which immediately yields a fully asymmetric eGH formulation eGH(f):

$$\langle A_n E_{n+1}\rangle_{\text{eGH}(f)} = \langle E_0\rangle\langle A_{n+1}\rangle + F_{tr}(n,n+1) \times (\langle A_n\rangle - \langle A_{n+1}\rangle) \text{ and} \tag{10a}$$

$$\langle E_n A_{n+1}\rangle_{\text{eGH}(f)} = \langle E_0\rangle\langle A_{n+1}\rangle. \tag{10b}$$

A less extreme but still asymmetric eGH formulation, eGH(a), anticipates weaker asymmetry upon relaxing the SFD constraint or for lower $\langle X_0\rangle$. We have confirmed this trend (not shown). In this case, we assume that deviations of pair probabilities from the MF results are proportional to the relevant A concentration, i.e., one assumes that $\Delta_n \propto \langle A_n\rangle$ and $\Delta_{n+1} \propto \langle A_{n+1}\rangle$ (cf. Fig. 2). This formulation yields

$$\langle A_n E_{n+1}\rangle_{\text{eGH}(a)} = 2\langle A_n\rangle\langle A_{n+1}\rangle\langle E_0\rangle/(\langle A_n\rangle + \langle A_{n+1}\rangle) + F_{tr}(n,n+1)\langle A_n\rangle(\langle A_n\rangle - \langle A_{n+1}\rangle)/(\langle A_n\rangle + \langle A_{n+1}\rangle) \text{ and} \tag{11a}$$

$$\langle E_n A_{n+1}\rangle_{\mathrm{eGH}(a)} = 2\langle A_n\rangle\langle A_{n+1}\rangle\langle E_0\rangle/(\langle A_n\rangle + \langle A_{n+1}\rangle) - F_{\mathrm{tr}}(n,n+1)\langle A_{n+1}\rangle(\langle A_n\rangle - \langle A_{n+1}\rangle)/(\langle A_n\rangle + \langle A_{n+1}\rangle). \quad (11b)$$

We note that for our application, results using (10) or (11), or even an alternative symmetric eGH formulation, eGH(s), where $\Delta_n = \Delta_{n+1}$ [33], are all much closer to precise model behavior determined by KMC simulation that the MF approximation.

B. Correlations impacting reaction kinetics

Next, we discuss analysis of the pair probabilities, $\langle A_n A_{n+1}\rangle$, which is necessary to describe the reaction kinetics, $R_n(C)$, in the evolution equations (3). The simplest treatment of reaction kinetics would simply apply a MF approximation $\langle A_n A_{n+1}\rangle \approx \langle A_n\rangle\langle A_{n+1}\rangle$. A simple hybrid approach might combine this MF treatment of reaction kinetics with a GH treatment of diffusion fluxes. A more refined approach would involve analysis of the evolution Eqs. (5) for $\langle A_n A_{n+1}\rangle$. This, in turn, requires analysis of the associated pair diffusion terms which involve quantities like $\langle A_n A_{n+1} E_{n+2}\rangle$, $\langle A_n E_{n+1} A_{n+2}\rangle$, and $\langle E_n A_{n+1} A_{n+2}\rangle$. The same argument as used above for pair probabilities and, as quantified in (8), suggests that these quantities will be much closer to each other than their MF estimates. Not only is this correct, but more sophisticated factorization approximations also fail to capture the key differences in these quantities. The reason for failure of such higher-order approximations is briefly discussed in Appendix C. Another relevant observation is that unlike the conventional diffusion flux terms appearing in the evolution equation for $\langle A_n\rangle$, one cannot readily adapt a hydrodynamic transport theory to reliably treat the unconventional pair diffusion flux terms appearing in the evolution equation for $\langle A_n A_{n+1}\rangle$. We will find that various treatments of the reaction kinetics of the above type produce qualitatively reasonable, but not quantitatively predictive results. Thus, we are motivated find an alternative strategy to assess $\langle A_n A_{n+1}\rangle$.

In fact, we resort to direct estimation of correlations associated with $\langle A_n A_{n+1}\rangle$ allowing treatment of reaction kinetics without analysis of the additional evolution equations for this quantity. To motivate our treatment, first we show KMC simulation results in Fig. 3 for SFD with $L = 100$, $\langle X_0\rangle = 0.8$ and $k/h = 0.001$ for $f_n = \langle A_n A_{n+1}\rangle/(\langle A_n\rangle\langle A_{n+1}\rangle)$, and also for $g_n = \langle A_n B_{n+1}\rangle/(\langle A_n\rangle\langle B_{n+1}\rangle)$, versus n, where deviations from unity reflect the strength of the spatial correlations. It is clear that values of $f_n > 1$ reflect clustering of A's which becomes particularly strong for increasing n. We emphasize that this clustering feature will significantly impact selectivity in reaction kinetics. In contrast, $g_n < 1$ values reflect anticlustering which is rather weak for intermediate n and becomes negligible for both large and small n [34].

The origin of the strong clustering of the A's deeper in the pore is somewhat subtle, so further discussion of this feature is appropriate (as well as of the weaker correlations between A's and B's). The rare event where A penetrates deep into the pore without reaction might be associated with density fluctuations near the pore openings, lower densities facilitating such transport. Clearly, if such a fluctuation facilitates transport of one A deep into the pore, it also facilitates transport of

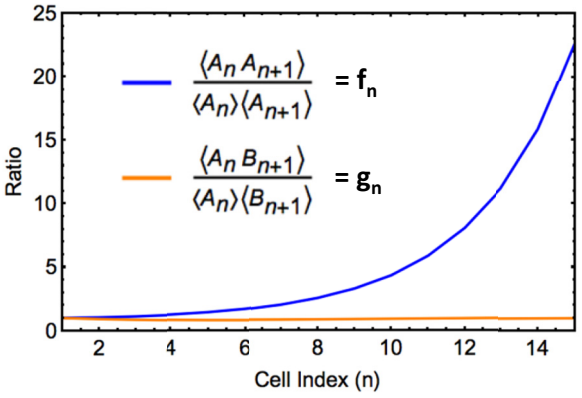

FIG. 3. KMC results for $f_n = \langle A_n A_{n+1}\rangle/(\langle A_n\rangle\langle A_{n+1}\rangle)$, $g_n = \langle A_n B_{n+1}\rangle/(\langle A_n\rangle\langle B_{n+1}\rangle)$, versus n near the left end of a pore with $L = 100$, $\langle X_0\rangle = 0.8$, $k/h = 0.001$, and $P_{\mathrm{ex}} = 0$ (SFD). Deviations from unity reflect the strength of the associated NN spatial correlation.

nearby pairs or larger groups of A. This feature explains the observed clustering of A's. However, this clustering is even more subtle in the sense the probability for a site n to be populated by A is enhanced not just by knowledge that site $n+1$ is populated by A (and more so if both $n+1$ and $n+2$ are populated by A), but it is also enhanced if it is known that site $n+2$ is populated by A and $n+1$ by B. For further discussion, see Appendix C. With regard to A-B correlations, most A deep in the pore will be isolated from each other and surrounded by a significant population of B's. There is no mechanism to induce significant positional correlations between these A and B species.

The above observations suggest the possibility of estimation of $\langle A_n A_{n+1}\rangle$ in the left half of the pore by using the exact relation $\langle A_n\rangle = \langle A_n A_{n+1}\rangle + \langle A_n B_{n+1}\rangle + \langle A_n E_{n+1}\rangle$, and then neglecting correlations in $\langle A_n B_{n+1}\rangle$, and also using (10a) or (11a) or alternative eGH expressions for $\langle A_n E_{n+1}\rangle$. Specifically, we set

$$\langle A_n A_{n+1}\rangle \approx \langle A_n\rangle - \langle A_n\rangle\langle B_{n+1}\rangle - \langle A_n E_{n+1}\rangle_{\mathrm{eGH}}. \quad (12)$$

Then $\langle A_n A_{n+1}\rangle$ in the right half of the pore is determined from the above results using symmetry about the pore center. In Table II, we show corresponding results for $f_n = \langle A_n A_{n+1}\rangle/(\langle A_n\rangle\langle A_{n+1}\rangle)$ for high concentration $\langle X_0\rangle = 0.8$ obtained from various eGH formulations. For SFD ($P_{\mathrm{ex}} = 0$), all eGH formulations capture the strong increase in f_n with increasing n, as determined precisely from KMC simulation. The fully asymmetric eGH formulation eGH(f), is most successful in capturing behavior up to $n = 10$. All formulations eventually increase more quickly than precise behavior, actually with eGH(f) deviating most. However, we find that it is primarily behavior for $n \leqslant 10$ which controls the reactive steady state, i.e., behavior deeper in the pore is not so relevant. From this perspective, eGH(f) is the most successful formulation as anticipated for SFD with high $\langle X_0\rangle$. For $P_{\mathrm{ex}} = 0.25$, correlations are far weaker, so any formulation gives reasonable results. As anticipated, eGH(a) performs slightly better than eGH(f). In Sec. IV, we shall see that (12) allows successful analytic treatment of behavior in the reactive steady state.

Finally, we have also analyzed behavior of f_n for $\langle X_0\rangle = 0.2$ (not shown). For SFD ($P_{\mathrm{ex}} = 0$), again f_n increases

TABLE II. f_n values for $\langle X_0\rangle = 0.8$ for three different eGH formulations: fully asymmetric choice (f) expected to be most appropriate for SFD and high $\langle X_0\rangle$, asymmetric choice (a), and simple symmetric choice (s). Results are shown for SFD ($P_{ex} = 0$) and $P_{ex} = 0.25$.

f_n values	$P_{ex} = 0.00$ eGH(s)	$P_{ex} = 0.00$ eGH(a)	$P_{ex} = 0.00$ eGH(f)	$P_{ex} = 0.00$ KMC	$P_{ex} = 0.25$ eGH(s)	$P_{ex} = 0.25$ eGH(a)	$P_{ex} = 0.25$ eGH(f)	$P_{ex} = 0.25$ KMC
$n = 1$	1.00693	1.00717	1.01385	1.01081	0.99563	0.99551	0.99125	1.00029
$n = 2$	1.01870	1.02004	1.03741	1.04782	0.99568	0.99556	0.99135	1.00037
$n = 3$	1.03618	1.04011	1.07235	1.12252	0.99551	0.99538	0.99101	1.00031
$n = 4$	1.06268	1.07160	1.12535	1.24534	0.99533	0.99520	0.99065	1.00015
$n = 5$	1.10838	1.12740	1.21676	1.42971	0.99519	0.99506	0.99039	1.00029
$n = 6$	1.18651	1.22442	1.37301	1.69431	0.99492	0.99478	0.98984	1.00010
$n = 7$	1.32613	1.40026	1.65225	2.06707	0.99469	0.99454	0.98939	0.99976
$n = 8$	1.57841	1.72113	2.15682	2.59594	0.99439	0.99423	0.98877	1.00000
$n = 9$	2.02822	2.29550	3.05643	3.34233	0.99414	0.99398	0.98829	0.99964
$n = 10$	2.84333	3.34063	4.68666	4.39688	0.99382	0.99364	0.98764	0.99930
$n = 11$	4.36949	5.31141	7.73897	5.89006	0.99350	0.99332	0.98700	0.99925
$n = 12$	7.18499	8.95460	13.36998	8.04207	0.99308	0.99288	0.98616	0.99892
$n = 13$	12.46148	15.80610	23.92296	11.10158	0.99275	0.99254	0.98549	0.99885
$n = 14$	22.13462	28.34838	43.26924	15.62479	0.99233	0.99212	0.98467	0.99938
$n = 15$	40.48814	52.25351	79.97628	22.42215	0.99204	0.99181	0.98407	0.99845

smoothly now from $f_1 = 1.003$ for $n = 1$ to $f_{15} = 1.421$ for $n = 15$ as determined from KMC simulation (a much slower increase than for $\langle X_0\rangle = 0.8$). In this case the eGH(a) predictions varying from $f_0 = 1.012$ to $f_{15} = 1.498$ match better precise KMC results than eGH(f) predictions varying from $f_0 = 1.024$ to $f_{15} = 1.948$. For $P_{ex} = 0.25$, spatial correlations are very weak and again eGH(a) is very effective.

IV. RESULTS FOR CONCENTRATION-DEPENDENT SELECTIVITY: $A \to B_c$ OR B_t

First, we present results for the steady-state concentration profiles for single-file diffusion (SFD with $P_{ex} = 0$) where spatial correlations are strongest, and effective analytic treatment is most difficult. Precise KMC simulation results in Fig. 4 for $L = 100$ and $\langle X_0\rangle = 0.8$ show that that $\langle A_n\rangle \approx 0$ in the center of the pore, and that the $\langle B_n^c\rangle$ and $\langle B_n^t\rangle$ profiles exhibit plateaus with nontrivial values subject to the constraint $\langle B_n^c\rangle + \langle B_n^t\rangle \approx \langle X_0\rangle$. This plateau behavior is somewhat less clear for $L = 100$ with significantly lower $\langle X_0\rangle = 0.2$, but would become quite clear for this $\langle X_0\rangle$ in longer pores.

Since B^t is preferentially created in regions with higher A concentration, one might have expected a bimodal profile for $\langle B_n^t\rangle$ (rather than a plateau) with peaks near the pore openings. Correspondingly, the profile for $\langle B_n^c\rangle$ would then be peaked in the pore center (since $\langle B_n^c\rangle + \langle B_n^t\rangle \approx \langle X_0\rangle$). While such transient behavior is found if starting with an initially empty pore (see Appendix E), it cannot be sustained in the steady state. The reason is simply that in the pore interior with no significant A population, concentration gradients in B^c and B^t are eventually eliminated by small but nonzero diffusion fluxes, $J_C(n > n+1) \approx -h\, F_{tr}(n,n+1)\nabla_n\langle C_{n+1}\rangle$ with $C = B^t$ and B^c.

We also show the predictions of the standard MF approximation and of our eGH formulations [using the GH approximation for diffusion fluxes, and (10a) or (11a) for $\langle A_n A_{n+1}\rangle$]. The standard MF approximation fails completely to capture concentration profile behavior. In contrast, the eGH formulations are particularly effective in capturing behavior even including the heights of the plateaus for individual B^c and B^t concentrations. More specifically, the eGH(f) formulation works especially well for higher $\langle X_0\rangle$ and the eGH(a) formulation for lower $\langle X_0\rangle$, as anticipated previously. To highlight the success of the eGH formulations, we emphasize that prediction of the values of the individual plateau concentrations is particularly delicate. We have explored various other "hybrid" treatments which use the GH approximation for diffusion fluxes, but either a MF treatment of reaction kinetics, or using other factorization approximations to treat pair diffusion fluxes. These produce qualitatively reasonable forms

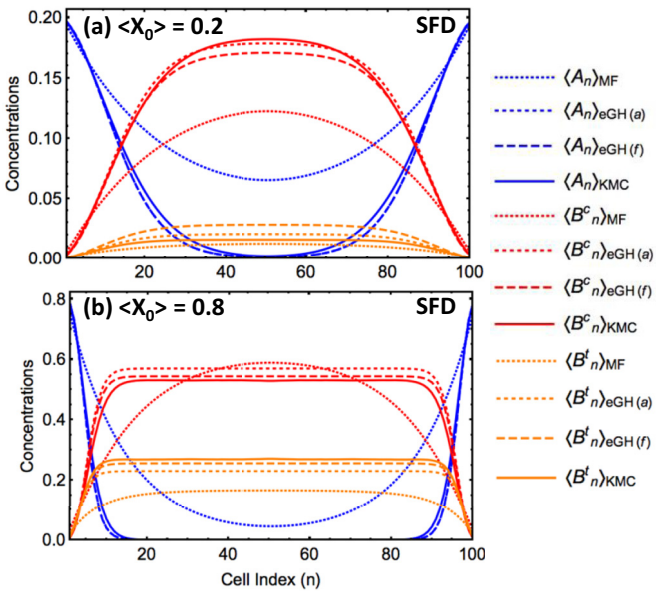

FIG. 4. Steady-state concentration profiles for SFD with $L = 100$ and $k/h = 0.001$: (a) $\langle X_0\rangle = 0.2$; (b) $\langle X_0\rangle = 0.8$. Comparison of precise behavior obtained from KMC simulation (solid curves) with poor MF predictions (dotted curves) and two successful eGH formulations (dashed curves).

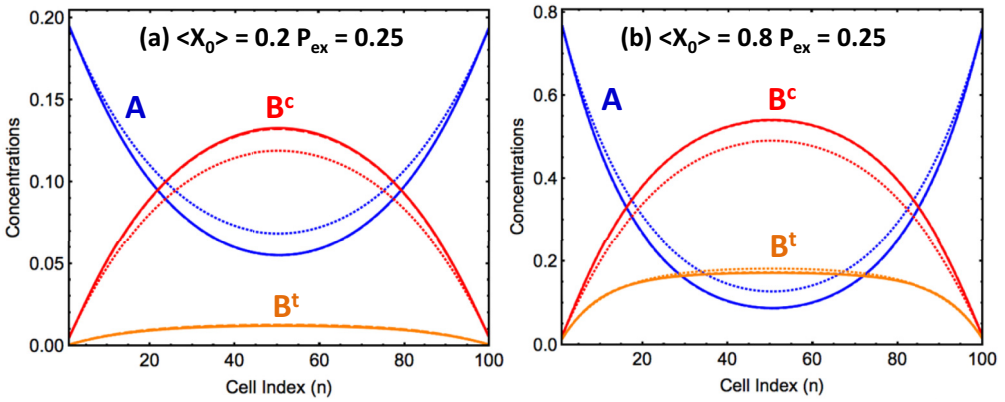

FIG. 5. Steady-state concentration profiles with exchange, $P_{ex} = 0.25$, for $L = 100$ and $k/h = 0.001$: (a) $\langle X_0 \rangle = 0.2$; (b) $\langle X_0 \rangle = 0.8$. Comparison of precise behavior obtained from KMC simulation (solid curves) with poor MF predictions (dotted curves). eGH formulations are effectively indistinguishable from precise behavior.

for concentration profiles, but do not have the quantitative predictivity of our eGH formulations. See Appendix D.

Next, we more briefly describe behavior when the SFD constraint is relaxed by selecting $P_{ex} = 0.25$. Here enhanced diffusion means greater reactant penetration into the pore, so longer pore lengths than $L = 100$ are needed to display a clear plateau in the pore center. Results for concentrations when $L = 100$ shown in Fig. 5 reveal that MF predictions (dotted curves) are significantly closer to precise behavior determined from KMC simulations (solid curves) than for SFD, although still not quantitatively precise. In contrast, predictions of our eGH formulations are effectively indistinguishable on these plots from the precise behavior.

Perhaps more significant than prediction of concentration profiles is the assessment of selectivity, i.e., determination of the relative yields of products B^c versus B^t. KMC simulation allows precise determination of the entire conversion rate profiles, $R_n(B^c)$ and $R_n(B^t)$, versus n. See Fig. 6 for results for SFD with $L = 100$, $k/h = 0.001$, and $\langle X_0 \rangle = 0.8$. Also shown are the results from a MF treatment, and from our analytic eGH(a) and eGH(f) treatments. The total conversion rates, $R_{tot}(B^{c,t}) = \sum_n R_n(B^{c,t})$, determine the selectivity through the ratio $\Re = R_{tot}(B^t)/R_{tot}(B^c)$. Analysis of behavior in Fig. 6 for SFD reveals that for $\langle X_0 \rangle = 0.8$, one has $\Re = 1.56$ from precise KMC analysis versus our best analytic eGH(f) estimate of $\Re = 1.40$, and the poor MF estimate of $\Re = 0.64$. For SFD with $\langle X_0 \rangle = 0.2$, one has $\Re = 0.171$ from KMC analysis versus our best eGH(a) estimate of $\Re = 0.181$, and the poorer MF estimate of $\Re = 0.135$. A more comprehensive comparison of KMC results with various analytic treatments are provided in Table III. As might be anticipated, eGH formulations reasonably recover precise behavior, but the MF treatment is inadequate particularly for higher $\langle X_0 \rangle$. Results are also given in Table III including exchange ($P_{ex} = 0.25$), where even the MF estimate is reasonable.

It is appropriate to provide further insight into the influence on selectivity of restricted diffusion (and particularly SFD), which impacts reactant concentration profiles, and of spatial correlations in the form of reactant clustering which impacts reaction kinetics. To this end, it is instructive to examine the value of $\Re$ determined by other simple treatments. In an alternative spatially coarse-grained description, one regards position in the pore as described by a continuous variable $x = na$ and the reactant concentration profile as a function

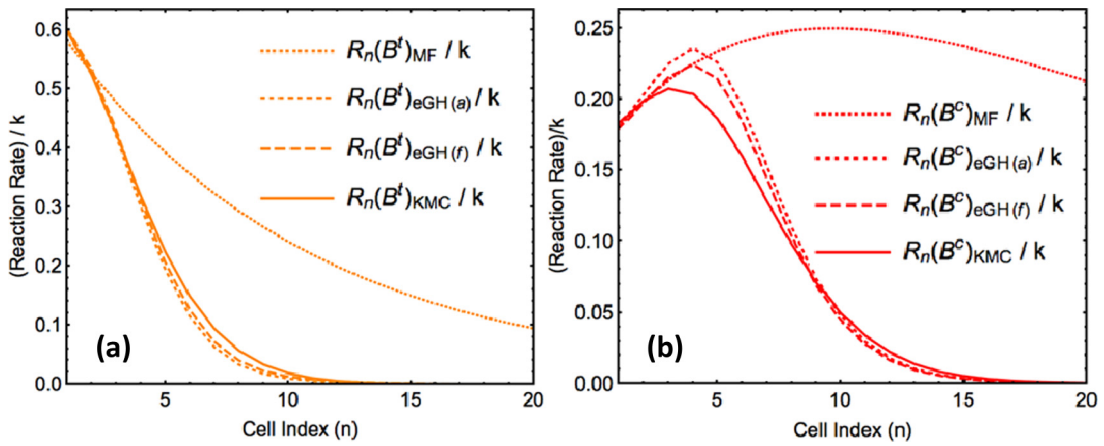

FIG. 6. Rescaled local production rates: (a) $R_n(B^c)/k$ and (b) $R_n(B^t)/k$ versus n near the left end of a pore with $L = 100$, $k = 0.001$ and $h = 1$, $\langle X_0 \rangle = 0.8$ (high concentration), and $P_{ex} = 0$ (SFD). Precise results from KMC (solid curves) are well described by our eGH formulations (dashed curves), but not by the MF approximation (dotted curves).

TABLE III. Selectivity, $\Re = R_{\rm tot}(B^t)/R_{\rm tot}(B^c)$, comparing precise value from KMC simulations [KMC] with predictions from the standard MF approximation [MF], a hybrid MF approximation [MF(H)], and various eGH formulations.

Analysis of $\Re$	$\langle X_0\rangle = 0.20$, $P_{\rm ex} = 0.00$	$\langle X_0\rangle = 0.80$, $P_{\rm ex} = 0.00$	$\langle X_0\rangle = 0.20$, $P_{\rm ex} = 0.25$	$\langle X_0\rangle = 0.80$, $P_{\rm ex} = 0.25$
KMC	0.1708	1.5579	0.1310	0.6917
MF	0.1347	0.6434	0.1368	0.7152
MF(H)	0.1476	1.1894	0.1311	0.6985
eGH(s)	0.1790	1.2876	0.1311	0.6913
eGH(a)	0.1806	1.3042	0.1336	0.6911
eGH(f)	0.2123	1.3950	0.1361	0.6842

of this continuous variable $\langle A(x)\rangle = \langle A_n\rangle$. In a MF treatment of reaction kinetics [factorizing expressions (2) for rates and coarse-graining], one has that

$$R_{\rm tot}(B^t) \approx k \int dx \langle A(x)\rangle^2$$

$$\text{and} \quad R_{\rm tot}(B^c) = k \int dx \langle A(x)\rangle[1 - \langle A(x)\rangle]. \qquad (13)$$

One can further show that for a MF treatment of diffusion, concentration profiles have exponential variation near the ends of a long pore so that $\langle A(x)\rangle \approx \langle X_0\rangle \exp[-(x/L_p)]$ near the left end of the pore where L_p denotes a penetration depth [7–9]. Then evaluation of integrals in (13) yields

$$\Re(\text{MF}) \approx \langle X_0\rangle/(2 - \langle X_0\rangle), \qquad (14)$$

so the maximum $\Re(\text{MF}) \approx 1$ occurs for $\langle X_0\rangle = 1$. For SFD with high $\langle X_0\rangle = 0.8$, this yields $\Re(\text{MF}) = 2/3 \approx 0.67$, far below the value above precise value of 1.56. (For SFD with $\langle X_0\rangle = 0.2$, one finds $\Re(\text{MF}) = 1/9 \approx 0.11$ also well below the precise value of 0.17.)

Next, we consider a hybrid treatment retaining MF reaction kinetics, but utilizing a GH formulation to account for the effect of SFD on the reactant concentration profile. If the GH tracer diffusion coefficient decays like $F_{\rm tr} \sim x^{-p}$ into the pore, then it has been shown that $\langle A(x)\rangle \approx \langle X_0\rangle \exp[-(x/L_p)^q]$ where $q = (2 + p)/2$ where we discuss the appropriate values of $p > 0$ and $q > 1$ below [2,10]. Note that MF behavior corresponds to $p = 0$ and $q = 1$. Evaluation of integrals in (13) now yields

$$\Re(\text{hybrid MF}) = \langle X_0\rangle/(2^{1/q} - \langle X_0\rangle). \qquad (15)$$

For SFD with high $\langle X_0\rangle = 0.8$, behavior is well described by the choice $p = 2$ and thus $q = 2$ [2,10], which yields $\Re(\text{hybrid MF}) \approx 1.30$ much closer to the precise value of 1.56 than the pure MF estimate for $q = 1$. However, a more appropriate hybrid MF treatment (see Appendix D), based on discrete evolution equations using a GH formulation for diffusion fluxes and MF treatment of reaction kinetics, obtains $\Re \approx 1.19$ not so close to the precise value. [For SFD with $\langle X_0\rangle = 0.2$, one finds an effective $p \approx 1$ corresponding to $q \approx 3/2$ [2,10]. This yields $\Re(\text{hybrid MF}) \approx 0.14$ improving over the simple MF estimate, but still below the precise value of 0.17.]

We conclude that deviations from a MF exponential reactant concentration profile are important in determining selectivity, but also clustering of reactants has a significant impact, particularly in producing higher $\Re$ values for SFD with high $\langle X_0\rangle$.

V. CONCLUSIONS

There is extensive interest within the statistical physics community in cooperative reaction-diffusion phenomena where traditional MF treatments of chemical kinetics and transport are inadequate [1,2]. Catalytic reactions in nanoporous materials with restrictive diffusive transport provide such an example where spatial correlations of kinetic origin invalidate MF assumptions. The additional feature of cooperative reaction kinetics, such as concentration- or environment-dependent selectivity considered here, constitutes an additional complication in the understanding and prediction of behavior. While KMC simulation of such reaction-diffusion models can reliably characterize such behavior, we show that for the system of interest here, an analytic formulation can be developed which provides deeper insight into the nature and role of subtle nonequilibrium spatial correlations in determining reaction behavior.

ACKNOWLEDGMENTS

We thank Sanjeevi Sivasankar for instructive comments on the form of concentration profiles inside the pore. This work was supported by the U.S. Department of Energy (USDOE), Office of Basic Energy Sciences, Division of Chemical Sciences, Geosciences, and Biosciences through the Ames Laboratory Chemical Physics program for the theory and modeling studies. The work was performed at Ames Laboratory which is operated for the USDOE by Iowa State University under Contract No. DE-AC02-07CH11358.

APPENDIX A: KMC SIMULATION ALGORITHMS

The basic principle of KMC simulation is to implement various processes (adsorption, desorption, diffusion, reaction) in the stochastic reaction-diffusion model with probabilities proportional to their physical rates. We first describe a rejection (rej) algorithm which is simpler to implement, but includes a fraction of failed attempts thus its reducing efficiency. One assigns a total rate $r_t = k + 6h$ for all types of processes at each cell in the pore (reaction plus hopping left or right of each of three types of species). The total rate, R_t(rej), for the system is r_t times the number of sites (taken as $L + 2$ since we must consider sites just outside the pore to treat adsorption). At each KMC step, simulation randomly picks sites and processes and attempts to implement (reaction is only implemented with probability k/r_t if the selected cell has an A; hopping right of B^c is only implemented with probability h/r_t if the selected cell has a B^c and the cell to the right is empty; etc.). The

simulation is run for $\sim 10^{11}$ KMC steps to be certain the steady state is reached, and then simulation data are collected for an additional $\sim 2 \times 10^{11}$ KMC steps.

A Bortz-type rejection-free (rf) algorithm maintains lists of the sets of particles which can be involved in each type of process (all n_A A's in the pore can react; the set of n_{Ar} A's with empty right NN cells which can hop right; etc.) The list must be updated after each simulation step, which requires extensive bookkeeping. Then the total rate of processes for the system is $R_t(\mathrm{rf}) = n_A k + n_{\mathrm{Ar}} h + \ldots$. Now one picks a type of process with probability proportional to its rate, i.e., $n_A\, k/R_t(\mathrm{rf})$, for reaction of A, picks a particle from the relevant list and implements the process for that particle. (For reaction, one would also have to select the product based on the local environment.) The simulation is run for $\sim 10^9$ KMC steps to equilibrate, and then data are collected for an additional $\sim 10^{10}$ KMC steps.

For our primarily focus on steady-state behavior, tracking of physical time in the simulation is not relevant. However, for studies of transient behavior (cf. Appendix D), time is incremented by $\Delta t = -\ln(w)/R_t$ at each Monte Carlo step where w is a random number uniformly distributed on [0,1].

APPENDIX B: MF ANALYSIS OF TRACER DIFFUSIVITY

It is possible to somewhat unconventionally assess tracer diffusivity, either at the MF-level or for higher-level approximations, from behavior of the concentration profiles in the steady state of our reaction-diffusion model [2,9]. This strategy exploits the feature noted Sec. II that the steady state corresponds to a counter diffusion mode where diffusion fluxes are proportional to the tracer diffusion coefficient in a hydrodynamic formulation. Here it suffices to take Eqs. (3) and (4) for $C = A$ and apply MF factorization. After substantial simplification, this equation reduces to

$$0 = d/dt\langle A_n\rangle = -k\langle A_n\rangle + (\langle E_0\rangle + P_{\mathrm{ex}}\langle X_0\rangle)h\nabla^2\langle A_n\rangle, \quad \text{(B1)}$$

where $\nabla^2\langle A_n\rangle = \langle A_{n+1}\rangle - 2\langle A_n\rangle + \langle A_{n-1}\rangle$ represents a discrete Laplacian. Since the coefficient in front of $\nabla^2\langle A_n\rangle$ corresponds to D_{tr}, we obtain $F_{\mathrm{tr}}(\mathrm{MF}) = \langle E_0\rangle + P_{\mathrm{ex}}\langle X_0\rangle$.

APPENDIX C: ANALYSIS OF MULTISITE CONFIGURATIONAL PROBABILITIES

The form of the "pair diffusion terms" in (5) motivates consideration and comparison of $\langle A_n A_{n+1} E_{n+2}\rangle$, $\langle A_n E_{n+1} A_{n+2}\rangle$, and $\langle E_n A_{n+1} A_{n+2}\rangle$. The same argument as used for $\langle A_n E_{n+1}\rangle$ and $\langle E_n A_{n+1}\rangle$ in Sec. III suggests that these triplet probabilities will be much closer than their MF values for SFD especially with high $\langle X_0\rangle$. This feature, which is confirmed in Fig. 7 for SFD with $\langle X_0\rangle = 0.8$ and $k/h = 0.001$, complicates the requirement of accurately describing differences in these quantities which constitute pair diffusion terms. Setting $\langle A_n A_{n+1} E_{n+2}\rangle - \langle A_n E_{n+1} A_{n+2}\rangle \approx \langle A_n\rangle(\langle A_{n+1} E_{n+2}\rangle - \langle E_{n+1}\rangle\langle A_{n+2}\rangle)$ would enable use of the GH approximation for the difference of pair probabilities. However, this crude factorization, denoted by (c) below, is not reliable. Also, as shown in the inset to Fig. 7, a standard pair approximation, denoted (pa) below, reliably describes

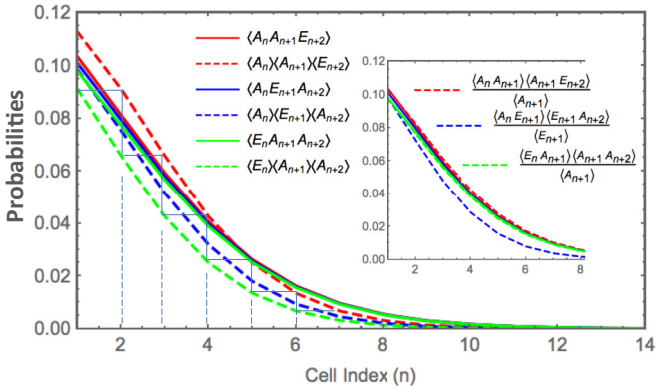

FIG. 7. Comparison of $\langle A_n A_{n+1} E_{n+2}\rangle$, $\langle A_n E_{n+1} A_{n+2}\rangle$, and $\langle E_n A_{n+1} A_{n+2}\rangle$ versus n determined precisely from KMC simulation and MF approximations near the left end of a pore for $L = 100$, $\langle X_0\rangle = 0.8$, $k/h = 0.001$, and $P_{\mathrm{ex}} = 0$ (SFD).

$\langle A_n A_{n+1} E_{n+2}\rangle$ and $\langle E_n A_{n+1} A_{n+2}\rangle$ in terms of pair quantities, but not $\langle A_n E_{n+1} A_{n+2}\rangle$. Thus, the pair approximation will fail to describe key differences in these quantities. The failure of the pair approximation for the quantity $\langle A_n E_{n+1} A_{n+2}\rangle$, and the failure of higher-order approximations for analogous probabilities involving four or more cells, is further elucidated by the conditional concentration analysis below.

Spatial correlations in the reactant distribution can be further elucidated by considering conditional reactant probabilities or concentrations $\langle A_n | C_{n+1} D_{n+2} \ldots\rangle = \langle A_n C_{n+1} D_{n+2} \ldots\rangle / \langle C_{n+1} D_{n+2} \ldots\rangle$ describing the probability that site n is occupied by A given that site $n+1$ is occupied by C, site $n+2$ is occupied by D, etc. In the absence of spatial correlations, one has that $\langle A_n | C_{n+1} D_{n+2} \ldots\rangle = \langle A_n\rangle$. Results are shown in Fig. 8 for SFD with $\langle X_0\rangle = 0.8$ and $k/h = 0.001$ for a substantial set of conditional reactant concentrations with one or two conditioning sites. These fall into distinct groups with values either above or below $\langle A_n\rangle$.

All of $\langle A_n | A_{n+1}\rangle$, $\langle A_n | A_{n+1} A_{n+2}\rangle$, $\langle A_n | A_{n+1} E_{n+2}\rangle$, $\langle A_n | E_{n+1} A_{n+2}\rangle$, $\langle A_n | A_{n+1} B_{n+2}\rangle$ and $\langle A_n | B_{n+1} A_{n+2}\rangle$ exceed $\langle A_n\rangle$, i.e., conditional reactant concentrations given one or more nearby A exceed $\langle A_n\rangle$. We also expect this feature to apply for conditional concentrations with more than two specified

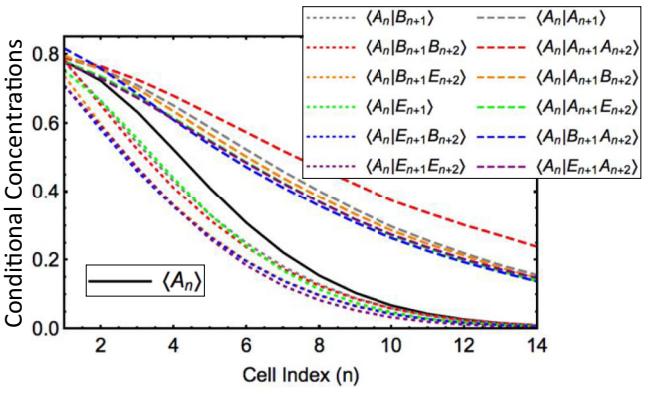

FIG. 8. Comparison of various conditional reactant concentrations versus n determined precisely from KMC simulation for $L = 100$, $\langle X_0\rangle = 0.8$, $k/h = 0.001$, and $P_{\mathrm{ex}} = 0$ (SFD).

cells. This feature indicates a subtle type of clustering corresponding to enhanced probabilities (relative to MF values) for configurations with an A on site n and one or more other A's on sites $n+1$ and $n+2$. The explanation of this behavior extends that used to rationalize the inequality $\langle A_n|A_{n+1}\rangle > \langle A_n\rangle$ in Sec. III. A density fluctuation near the pore opening reducing the density could facilitate diffusion of A and of clusters of A deeper into the pore. Then it follows that $\langle A_n|A_{n+1}\rangle$, $\langle A_n|A_{n+1}B_{n+2}\rangle$, $\langle A_n|E_{n+1}A_{n+2}\rangle$, etc., exceed $\langle A_n\rangle$. It is perhaps less clear why $\langle A_n|B_{n+1}A_{n+2}\rangle > \langle A_n\rangle$, but consider a triple of A's diffusing deep into the pore (aided by a density fluctuation) where the central A reacts to convert to B. This scenario can lead to formation of $A_nB_{n+1}A_{n+2}$ configurations.

Next, we note that both $\langle A_n|E_{n+1}\rangle$ and $\langle A_n|E_{n+1}E_{n+2}\rangle$ are below $\langle A_n\rangle$. These results are equivalent to the inequalities $\langle A_nE_{n+1}\rangle < \langle A_n\rangle\langle E_{n+1}\rangle$ and $\langle A_nE_{n+1}E_{n+2}\rangle < \langle A_n\rangle\langle E_{n+1}E_{n+2}\rangle = \langle A_n\rangle\langle E_{n+1}\rangle\langle E_{n+2}\rangle$ (the latter equality following since empty cells are randomly distributed). These inequalities have been explained at the beginning of Sec. III, where we note that values of $\langle A_nE_{n+1}\rangle$ and $\langle E_nA_{n+1}\rangle$ are close, as are those of $\langle A_nE_{n+1}E_{n+2}\rangle$, $\langle E_nA_{n+1}E_{n+2}\rangle$, and $\langle E_nE_{n+1}A_{n+2}\rangle$ (due to the facile diffusion of A between the indicated pair or triple of sites). Our resulting understanding of the contrasting behavior of $\langle A_n|E_{n+1}\rangle < \langle A_n\rangle$ and of $\langle A_n|E_{n+1}A_{n+2}\rangle > \langle A_n\rangle$ explains the failure of the standard pair approximation to treat $\langle A_nE_{n+1}A_{n+2}\rangle$ and thus to treat pair diffusion fluxes in the evolution equation for $\langle A_nA_{n+1}\rangle$ (cf. Sec. III).

Finally, we note that all of $\langle A_n|B_{n+1}\rangle$, $\langle A_n|B_{n+1}B_{n+2}\rangle$, $\langle A_n|B_{n+1}E_{n+2}\rangle$, and $\langle A_n|E_{n+1}B_{n+2}\rangle$ are also below $\langle A_n\rangle$, but also that these quantities approach $\langle A_n\rangle$ for large n where the associated correlations are diminished deeper in the pore.

APPENDIX D: HYBRID APPROXIMATIONS

We have seen that a standard MF approximation applied to treat both diffusion fluxes and reaction kinetics fails dramatically to describe reactant penetration into the pore for small P_{ex} and small k [10]. However, a GH formulation of diffusion fluxes yields reliable description of the reactant concentration profile. Thus, it remains only to treat the reaction kinetics in order to describe behavior of the $A \to B^c$ or B^t conversion reaction. Here we first consider the simplest hybrid formulation, MF(H), using a GH treatment of diffusion fluxes and a MF treatment of reaction kinetics (i.e., ignoring spatial correlations in the reactant distribution). MF(H) results for steady-state concentration profiles shown in Fig. 9 for SFD with $\langle X_0\rangle = 0.8$ qualitatively reproduce KMC simulation behavior. However, predictions for plateau concentrations of B^c and B^t differ significantly from the precise values, in contrast our eGH formulation accounting for reactant clustering. As noted in Table III, one obtains $\Re = 1.19$ for MF(H) versus $\Re = 1.40$ for eGH(f) versus the precise value of $\Re = 1.56$ from KMC simulation.

We have implemented other hybrid formulations which retain the GH treatment of diffusion flux in the equations for single-cell concentrations, but apply various factorization approximations to the pair diffusion fluxes in the evolution equations for $\langle A_nA_{n+1}\rangle$. We have applied a crude factorization (c), e.g., $\langle A_nA_{n+1}E_{n+2}\rangle - \langle A_nE_{n+1}A_{n+2}\rangle \approx \langle A_n\rangle(\langle A_{n+1}E_{n+2}\rangle - \langle E_{n+1}\rangle\langle A_{n+2}\rangle)$, and then used the GH treatment of the second factor. Fig. 9 also reveals that for

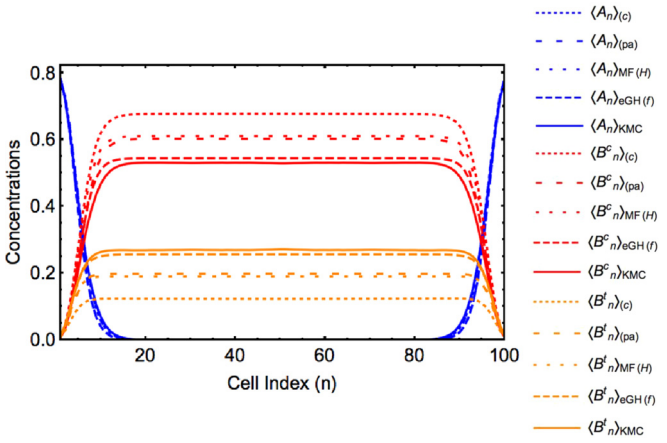

FIG. 9. Comparison of various hybrid approximations, including MF(H) and a crude factorization of pair diffusion terms (c) and a pair factorization (pa) with precise behavior (KMC) and our eGH(f) treatment for $L = 100$, $\langle X_0\rangle = 0.8$, $k/h = 0.001$, and $P_{ex} = 0$ (SFD).

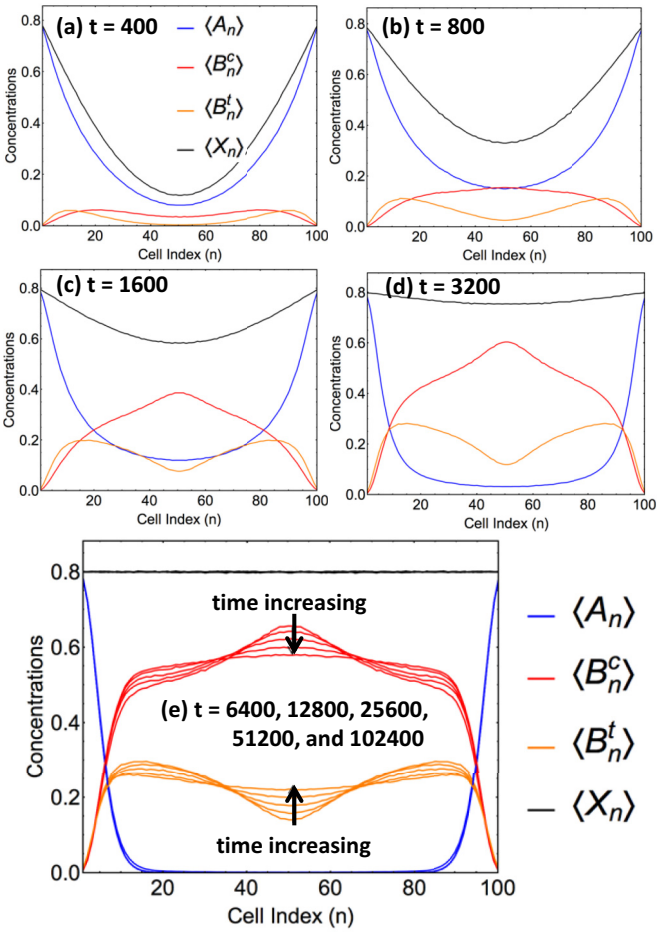

FIG. 10. KMC simulation results for the evolution of concentration profiles starting from an empty pore for $L = 100$, $\langle X_0\rangle = 0.8$, and $k/h = 0.001$. Times are indicated (in units where $h = 1$) and increase from panels (a) to (e).

SFD with $\langle X_0\rangle = 0.8$, predictions of this approach (c) while qualitatively reasonable actually give a poorer estimate of plateau concentrations even than the hybrid MF approach. As another alternative denoted (pa), we have implemented a standard pair factorization for the pair diffusion terms and then used the eGH approximation to describe $\langle A_n E_{n+1}\rangle$ and $\langle E_{n+1} A_n\rangle$ terms. Recall that we know from Appendix B that the pair approximation is inadequate for $\langle A_n E_{n+1} A_{n+2}\rangle$. This approach predicts concentration profiles very similar to the MF(H) prediction for SFD with $\langle X_0\rangle = 0.8$, and thus again deviating significantly from precise results in contrast to our eGH approach. See Fig. 9.

APPENDIX E: TRANSIENT BEHAVIOR WITH AN INITIALLY EMPTY PORE

We have performed simulations to characterize evolution of concentration profiles starting with an initially empty pore for $L = 100$, $\langle X_0\rangle = 0.8$, and $k/h = 0.001$. See Fig. 10. The key features are as follows. The quasi-steady-state reactant profile develops relatively quickly on the times scale of pore filling, where the filling process takes a time $t_f \sim 2000$ (in units of $1/h$) to achieve a roughly constant total concentration of $\langle X_n\rangle \approx 0.8$. This time scale follows from Einstein's relation $(L/2)^2 \sim h\, t_f$ since particles must diffuse a length $\sim L/2$ to fill the pore. At the end of this filling stage, B^t has a bimodal profile peaked towards the pore openings, and the B^c profile is peaked in the pore center. The second stage of evolution to achieve the true steady state, where both B^c and B^c profiles exhibit plateaus in the pore center, takes much longer around $t_{ss} \sim 10^5$. This much slower time scale is understood since such evolution is controlled by the magnitude of the tracer diffusion coefficient $F_{tr}(n, n+1) \approx (1 - \langle X_0\rangle)(\langle X_0\rangle)^{-1}/L \approx 0.0025$ in the pore center [35]. Diffusion over a length scale of $\sim$20 cells would only occur on a time scale of $\sim t_{ss}$ given such a low diffusion coefficient.

[1] Chemical kinetics beyond the textbook: Fluctuations, many-particle effects and anomalous dynamics, J. Phys.: Condens. Matter **19**(6) (2007), Special Issue edited by K. Lindenberg, G. Oshanin, and M. Tachiya.

[2] D.-J. Liu, A. Garcia, J. Wang, D. M. Ackerman, C.-J. Wang, and J. W. Evans, Chem. Rev. **115**, 5979 (2015).

[3] J. G. Tsikoyiannis and J. E. Wei, Chem. Eng. Sci **46**, 233 (1991).

[4] C. Rodenbeck, J. Kärger, and K. Hahn, J. Catal. **157**, 656 (1995).

[5] C. Rodenbeck, J. Kärger, and K. Hahn, Phys. Rev. E **55**, 5697 (1997).

[6] M. S. Okino, R. Q. Snurr, H. H. Kung, J. E. Ochs, and M. L. Mavrovouniotis, J. Chem. Phys. **111**, 2210 (1999).

[7] S. V. Nedea, A. P. J. Jansen, J. J. Lukkien, and P. A. J. Hilbers, Phys. Rev. E **65**, 066701 (2002).

[8] S. V. Nedea, A. P. J. Jansen, J. J. Lukkien, and P. A. J. Hilbers, Phys. Rev. E **66**, 066705 (2002).

[9] D. M. Ackerman, J. Wang, J. H. Wendel, D.-J. Liu, M. Pruski, and J. W. Evans, J. Chem. Phys. **134**, 114107 (2011).

[10] D. M. Ackerman, J. Wang, and J. W. Evans, Phys. Rev. Lett. **108**, 228301 (2012).

[11] J. Wang, D. M. Ackerman, V. S.-Y. Lin, M. Pruski, and J. W. Evans, J. Chem. Phys. **138**, 134705 (2013).

[12] T. E. Harris, J. Appl. Prob. **2**, 323 (1965).

[13] M. Kollmann, Phys. Rev. Lett. **90**, 180602 (2003).

[14] F. Marchesoni and A. Taloni, Phys. Rev. Lett. **97**, 106101 (2006)

[15] K. Manna, N. Eedugurala, and A. D. Sadow, J. Am. Chem. Soc. **137**, 425 (2015).

[16] F. J. M. M. de Gauw, J. van Grondelle, and R. A. van Santen, J. Catal. **204**, 53 (2001).

[17] Z. Karpinski, S. N. Gandhi, and W. M. H. Sachtler, J. Catal. **141**, 337 (1993).

[18] L. Heinke and J. Kärger, Phys. Rev. Lett. **106**, 074501 (2011).

[19] B. G. Trewyn, I. I. Slowing, S. Giri, H. T. Chen, and V. S.-Y. Lin, Accounts Chem. Res. **40**, 846 (2007).

[20] K. Kandel, S. M. Althaus, C. Peraphatdit, B. G. Trewyn, M. Pruski, and I. I. Slowing, J. Catal. **291**, 63 (2012).

[21] K. Manna, W. S. Everett, G. Schoendorff, A. Ellern, T. L. Windus, and A. D. Sadow, J. Am. Chem. Soc. **135**, 7235 (2013).

[22] N. Eedugurala, Z. R. Wang, U. Chaudhary, N. Nelson, K. Kandel, T. Kobayashi, I. I. Slowing, M. Pruski, and A. D. Sadow, ACS Catal. **5**, 7399 (2015).

[23] W. C. Everett, J. W. Evans, A. D. Sadow, and T. L. Windus (unpublished).

[24] A. Klamt and G. Schuurmann, J. Chem. Soc., Perkin Trans. **2**, 799 (1993).

[25] M. Cossi, N. Rega, G. Scalmani, and V. Barone, J. Comput. Chem. **24**, 669 (2003).

[26] D. S. Sholl, Acc. Chem. Res. **39**, 403 (2006).

[27] K. Malek, T. J. H. Vlugt, and B. Smit, in *Catalysis and Materials Science*, edited by R. A. van Santen and P. Sautet (Wiley-VCH, Weinheim, 2009), Chap. 14.

[28] C.-J. Wang, D. M. Ackerman, I. I. Slowing, and J. W. Evans, Phys. Rev. Lett. **113**, 038301 (2014).

[29] P. H. Nelson and S. M. Auerbach, Chem. Eng. J. **74**, 43 (1999).

[30] H. Spohn, *Large Scale Dynamics of Interacting Particles* (Springer, Berlin, 1991).

[31] J. Quastel, Commun. Pure Appl. Math. **45**, 623 (1992).

[32] The mean residence time of an A in the pore at site $n+1$, and such an A given site n is E, are expected to be similar. The mean residence time of A at n is likely below that of A at n given site $n+1$ is E. In the latter case, the A at n could have likely explored site $n+1$ previously indicating that it has been in the pore longer. The probability for conversion of A to B naturally increases with residence time [5].

[33] The symmetric version of the eGH approximation, eGH(s), yields $\langle A_n E_{n+1}\rangle_{\text{eGH(s)}} \approx {}^1\!/_2(\langle A_n\rangle + \langle A_{n+1}\rangle)\langle E_0\rangle + {}^1\!/_2 F_{tr}(n,n+1)(\langle A_n\rangle - \langle A_{n+1}\rangle)$ and $\langle E_n A_{n+1}\rangle_{\text{eGH(s)}} \approx {}^1\!/_2(\langle A_n\rangle + \langle A_{n+1}\rangle)\langle E_0\rangle - {}^1\!/_2 F_{tr}(n,n+1)(\langle A_n\rangle - \langle A_{n+1}\rangle)$.

[34] We find similar strength of weak AA-clustering and weak AB-anticlustering near the pore opening. Setting $g_n = 1/f_n$ leads to some improvement in estimates of f_n for $n \approx 1$–4, but fails completely for larger n.

[35] D.-J. Liu, J. Wang, D. M. Ackerman, I. I. Slowing, M. Pruski, H.-T. Chen, V. S.-Y. Lin, and J. W. Evans, ACS Catal. **1**, 751 (2011).